JOURNAL OF NANO- AND ELECTRONIC PHYSICS
Vol. 17 No 1, 01002(7pp) (2025)

ЖУРНАЛ НАНО- ТА ЕЛЕКТРОННОЇ ФІЗИКИ
Том 17 № 1, 01002(7cc) (2025)

OPEN ACCESS

REGULAR ARTICLE

Effect of SiN_x/SiO_2 Passivation Layers on Diffused Front Surface Field in *n*-type Silicon Wafers

B. Labdelli[1,*], A. Boucheham[1], L. Benharrat[1], A. Djelloul[1,†], N. Chahinez[1], M. Alloun[2], S.Y. Lamri[2]

[1] *Centre de Recherche en Technologie des Semi-Conducteurs pour l'Energétique 'CRTSE', Alger, Algérie*
[2] *École Nationale Polytechnique Département de Métallurgie, 16200 Alger, Algeria*

(Received 03 December 2024; revised manuscript received 12 February 2025; published online 27 February 2025)

In this research, the passivation properties of a stack of silicon nitride (SiN_x) films over silicon dioxide (SiO_2) on *n*-type Si wafers to study its effect on the Front Surface Field (FSF) in PERT solar cells were investigated. The silicon wafers underwent an identical thermal oxidation process for 30 min at 850 °C (10 nm) in an oxidation oven. SiN_x materials have been deposited by Plasma Enhanced Chemical Vapor Deposition (PECVD) on an *n*-type Silicon substrate, silicon nitride, where precursor gas ratios ($R = NH_3/SiN_4$) are adjusted, then Rapid thermal processing (RTP) co-firing at a temperature of 750 °C for 60 s was used. Where the phosphorus diffusions are done using $POCl_3$ as a dopant source at a temperature of 820 °C for 15 min in a tube furnace. The reflecting index shows that the double layers of SiN/SiO_2 films in the solar cells allow the antireflection effects, and the good passivation of the emitters has led to better electrical performance, which was confirmed using the Sinton WCT 120 quasi-steady state photo-conductance (QSSPC) using $n^+/n/n^+$ symmetrical lifetime samples. The SiN_x layers that are deposited on SiO_2 exhibit superior bulk and surface passivation characteristics.

Keywords: SiN_x/SiO_2, PECVD, RTP, *n*-type monocrystalline silicon, QSSPC.

DOI: 10.21272/jnep.17(1).01002

PACS numbers: 82.65. + r, 81.15.Gh, 61.72.Cc, 61.72.uf, 07.60. – j

1. INTRODUCTION

Passivated Emitter and Rear Totally Diffused (PERT) solar cell is a member of Passivated Emitter and Rear Contact (PERC) family, *n*-type PERT is considered a promising candidate in photovoltaics (PV). When combined with homogeneous FSF, PECVD SiO_x may successfully stop the SRH surface recombination and prevent light-induced deterioration (LID) of *n*-PERT [1, 2]. One common problem with surface passivation employing plasma SiN_x films is the comparatively low stability of the passivation quality during the annealing procedure [2]. A substantial lifetime increase was observed by depositing SiN_x on the top of SiO_2 layer [3, 4]. Passivation of the front and rear surfaces is considered an effective approach for enhancing the electrical performance of the manufactured cells. In addition to reducing reflection losses, surface passivation for diffused n^+ emitters and hydrogen passivation of bulk defects are simultaneously provided by amorphous SiN_x films produced by plasma-enhanced chemical vapor deposition (PECVD) [5, 6]. This work aims to clarify the impact of SiN_x/SiO_2 double-passivation layer on *n*-type mono-crystalline silicon wafers (*n*-type Si) paving. The way for the production of efficient solar cells. *n*-type Si wafers have several advantages, as numerous studies have demonstrated their high resistance, high tolerance to metallic impurities, and reduced light-induced degradation caused by B-O complexes [7-11]. The international technology roadmap for photovoltaics (ITRPV) predicted that monocrystalline *n*-type Si substrates will account for more than > 30 % of the global market over the next ten years [12]. Three distinct crystallographic structures of stochiometric (Si_3N_4), known as (α, β, and γ) phases, exist [13]. By adjusting the N/Si ratio of the films, it is possible to customize the refractive index of α-SiN_x [14]. The SiO_2/SiN_x double layer is more thermally stable than SiN_x monolayers, which show degradation after thermal annealing. Such SiN_x/Si interfaces can increase passivation quality by introducing a thin oxide layer [15]. In this work, a double-passivation layer of SiN_x/SiO_2 was deposited on Cz-Si (*n*) wafers with a symmetrical emitter structure ($n^+/n/n^+$). Effective carrier lifetime was determined using quasi-steady state photo-conductance (QSSPC) to assess the quality of the passivated wafers. The optical properties of the pre-pared double-passivation layers were also investigated. Further properties as quantities of elements present on the surface were analyzed using

[*] Correspondence e-mail: boutaleb200574@yahoo.fr
[†] djelloulcrtse@gmail.com

© 2025 The Author(s). Journal of Nano- and Electronic Physics published by Sumy State University. This article is distributed under the terms and conditions of the Creative Commons Attribution (CC BY) license.

Cite this article as: B. Labdelli et al., *J. Nano- Electron. Phys.* 17 No 1, 01002 (2025) https://doi.org/10.21272/jnep.17(1).01002

X-ray photoelectron spectroscopy (XPS), SEM examination in conjunction with cross-sectional analysis (EDS) was carried out to examine the surface morphology.

2. EXPERIMENTAL DETAILS

2.1 Material and Methods

Czochralski-grown (CZ) *n*-type monocrystalline Si wafers (4-inch size) were used to produce $n^+/n/n^+$ structures with 1-3 Ω·cm base resistivity, and a thickness of ~ 360 µm. After the Piranha etching procedure (Fig. 1), the nn^+ junction was created by diffusing phosphorus oxychloride ($POCl_3$) at 820 °C for 15 minutes. After diffusion process, phosphorus silicate glass (PSG) was removed by dipping in HF. All the samples were rinsed in deionized water and dried. Using the flow of gas N_2/O_2 at 850 °C, a thermal oxidation porous was achieved in a quartz tube furnace for 30 min; in the second step, SiN_x:H films were deposited using silane (SiH_4) and ammonia (NH_3) as precursor gases with variable flow ratios of 4, 5, 6.5, and 8 deposited at low temperatures of 380 °C in a PECVD reactor from SEM-CO Engineering, followed by Rapid thermal processing (RTP) at a temperature of 750 °C for 60 seconds. N_1, N_2, N_3, and N_4 refer to the samples prepared at $R = 4$, 5, 6.5 and 8 ratios, respectively. Using a UV-Visible spectrophotometer Cary 500, reflectance measurements were performed for the SiN_x/SiO_2 double-layer. The Fourier transformed infrared (FTIR) spectroscopy.

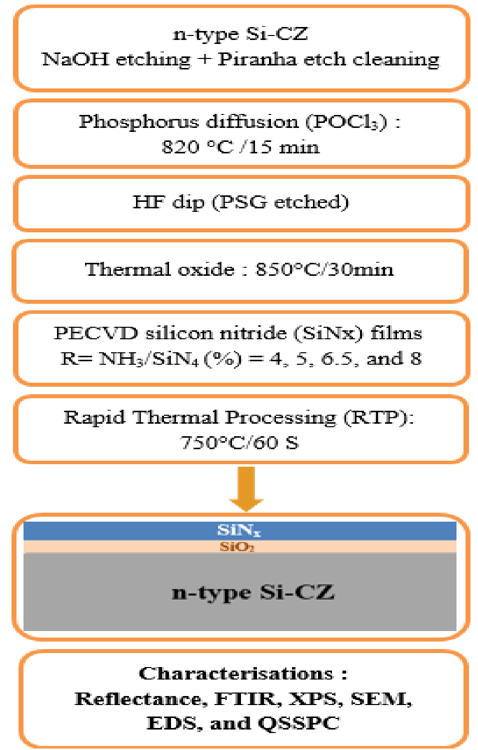

Fig. 1 – Flow chart of fabrication of symmetrical $n^+/n/n^+$ structures

Thermo Nicolet NEXUS 670 was used in the $400 - 4000\ cm^{-1}$ range to identify the bonding characteristics of the layers. The X-ray photoelectron spectroscopy (XPS) Escalab Xi^+ depth profiling allows us to deter-mine the nature of the chemical elements present on the surface of our samples. The morphology of the SiN_x/SiO_2 layer surfaces is determined from scanning electron microscope (SEM) JSM7610F Plus images. Peak intensities measured by Energy Dispersive Spectroscopy (EDS), are used in quantitative analysis to determine the concentration of a particular element in a sample. The Sinton Instruments photo-conductance decay tester (WCT-120) was used to measure the effective lifetime of symmetrical $n^+/n/n^+$ structures [16], with a quasi-steady-state photo-conductance (QSSPC) tool.

2.2 Characterization

The characterization techniques used were mainly four-point probe (CMT-SR2000N, Chang-Min Co, Ltd., 2000) to measure the resistivity, quasi-steady-state photo-conductance (QSSPC) for life-time measurements, scanning electron microscopy (SEM) and energy dispersive spectrometer (EDS) for morphology and chemical composition analysis, electrochemical capacitance-voltage (ECV) profiler PN 4300-PC and secondary ion mass spectroscopy (SIMS) to perform doping profile measurements.

3. RESULT AND DISCUSSION

3.1 Reflectance Measurements

The reflectivity of some double-layer SiO_2/SiN_x films at a wavelength ranging from 611 nm to 780 nm, using reflectance measurements with different gas flow coefficients ($R = NH_3/SiN_4$), is presented in Fig. 2.

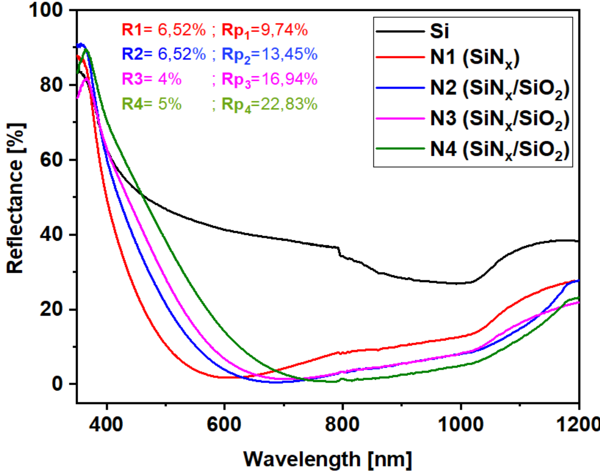

Fig. 2 – Reflectivity of SiN_x/SiO_2 double layer with different gas flow coefficients ($R = NH_3/SiN_4$)

The weighted average reflectance value is deter-mined using Eq. 1, [17]:

$$R_p = \frac{\int_{\lambda_1}^{\lambda_2} R(\lambda)\phi(\lambda)d(\lambda)}{\int_{\lambda_1}^{\lambda_2} \phi(\lambda)d(\lambda)} \quad (1)$$

Where $R(\lambda)$ is the reflectance measured of the solar cell for the corresponding wavelength λ and $\varphi(\lambda)$ is the spectral irradiance of the solar spectrum AM 1.5G. The thickness of the double layer was also calculated from the following law [17]:

$$d = \frac{\lambda_{\min}}{4n} \quad (2)$$

where "d" represents the thickness of the layer, "λ" is the wavelength of the incident light, and "n" is the refractive index of the layer material.

Table 1 – Calculated weighted reflections R_p of different passivation layers

Samples	Passivation layers	Weighted R_p	R_{min}	λ_{min}
N1	SiN_x	9.74	1.672	611
N2	SiN_x/SiO_2	13.45	0.493	686
N3	SiN_x/SiO_2	16.97	1.297	709
N4	SiN_x/SiO_2	22.83	0.688	783

Fig. 3 below shows the relationship between reflectance and SiN_x/SiO_2 thickness. A thin oxide/nitride stack offers surface passivation marginally superior to the best single-layer SiN_x passivation. We used equation number 2 to see that, Si_3N_4 thickness is varied from 65 nm to 90 nm, and no interlayers exist between Si_3N_4 and Si. Higher values for k cause the layers to become lighter absorbing, and the lower the value for R, the higher the value for the refractive index [18].

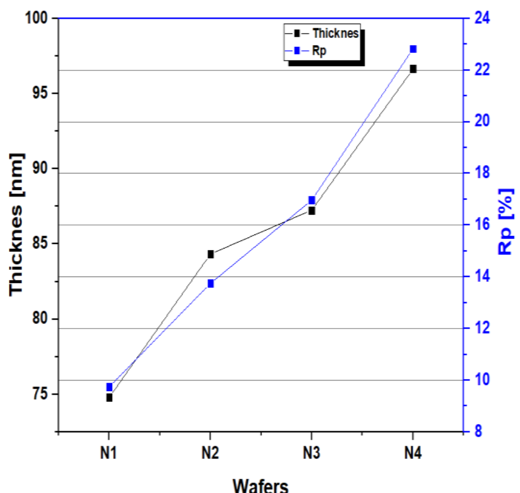

Fig. 3 – Weighted reflectance (in %) and mutual SiN_x thicknesses (nm)

However, the much increased thermal stability of the surface passivation provided by the thin oxide/nitride stacks compared to the single-layer SiN_x passivation is even more significant [19]. Lauinger T et al., found that the comparatively low stability of the passivation quality during annealing treatments is a common issue with surface passivation employing plasma SiN films [20].

3.2 FTIR Characterization

Fig. 4 depicts the FTIR spectrum of the SiN_x/SiO_2 double-layer measured on of N_4 sample. The presence of bonds of interstitial impurities of carbon originating from the elaboration is observed, in addition to the bonds of Si-O and Si-N predicted by our experiment, due to the deposition of nitride and thermal oxidation.

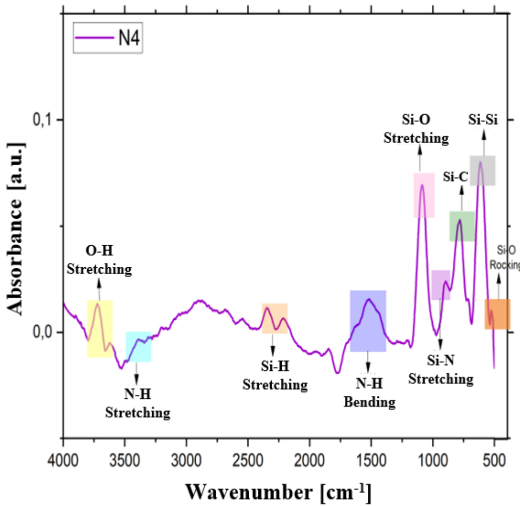

Fig. 4 – Spectrum of absorbance of N_4 sample as a function of wave number

In various vibrational modes, a substantial number of distinct hydrogen bonds, whether Si-H, O-H, or N-H, are also observed. Although FTIR cannot quantify the exact amounts of hydrogen content, it can represent a decent approximation of the bonding structure. An FTIR, simply reveals the material's bonded amount of hydrogen. In addition to the little proportion caused by the elaboration of the silicon, carbon Si-C (carbonaceous residues are found at peaks at specific places due to contamination by the CH_3 present in the air) contamination is seen. The temperature of 750 °C was considered a critical temperature since the amorphous silicon nitride thin films are often subjected to thermal processes including rapid thermal annealing for metal contact firing at this temperature. One may suggest that after a Rapid Thermal Processing (RTP) process at high temperatures (over 700 °C), the Si-H peak is not eliminated and the N-H peak is 30 % of the total hydrogen content. We conclude that the hydrogen releases from SiN_x during the RTA annealing process.

3.3 XPS Characterization

This technique offers a comprehensive understanding of the types and quantities of elements present on a given

surface. In this respect, we display in Fig. 5 (a), the XPS survey spectra of SiO_2, N_2, N_3, and N_4 samples. The core level photoelectron peaks, namely Si 2*p*, N 1*s*, O 1*s*, and C 1*s*, corresponding to silicon, nitrogen, oxygen, and carbon, respectively, are discernible in the figure 5. Additionally, the Fig. 6 depicts also the peaks associated with C KLL, N KLL, and O KLL Auger transitions, which are linked to carbon, nitrogen, and oxygen elements. The atomic percentages [at. %] of N, Si, O, and C elements are derived from the signals of N 1*s*, Si 2*p*, O 1*s*, and C 1*s*, respectively.

These calculations are succinctly presented in the table included in Fig. 6 (a). To facilitate comparison, these atomic percentages are then graphically represented in Fig. 6 (b). This visualization enables a clear and concise understanding of the elemental composition across the different samples.

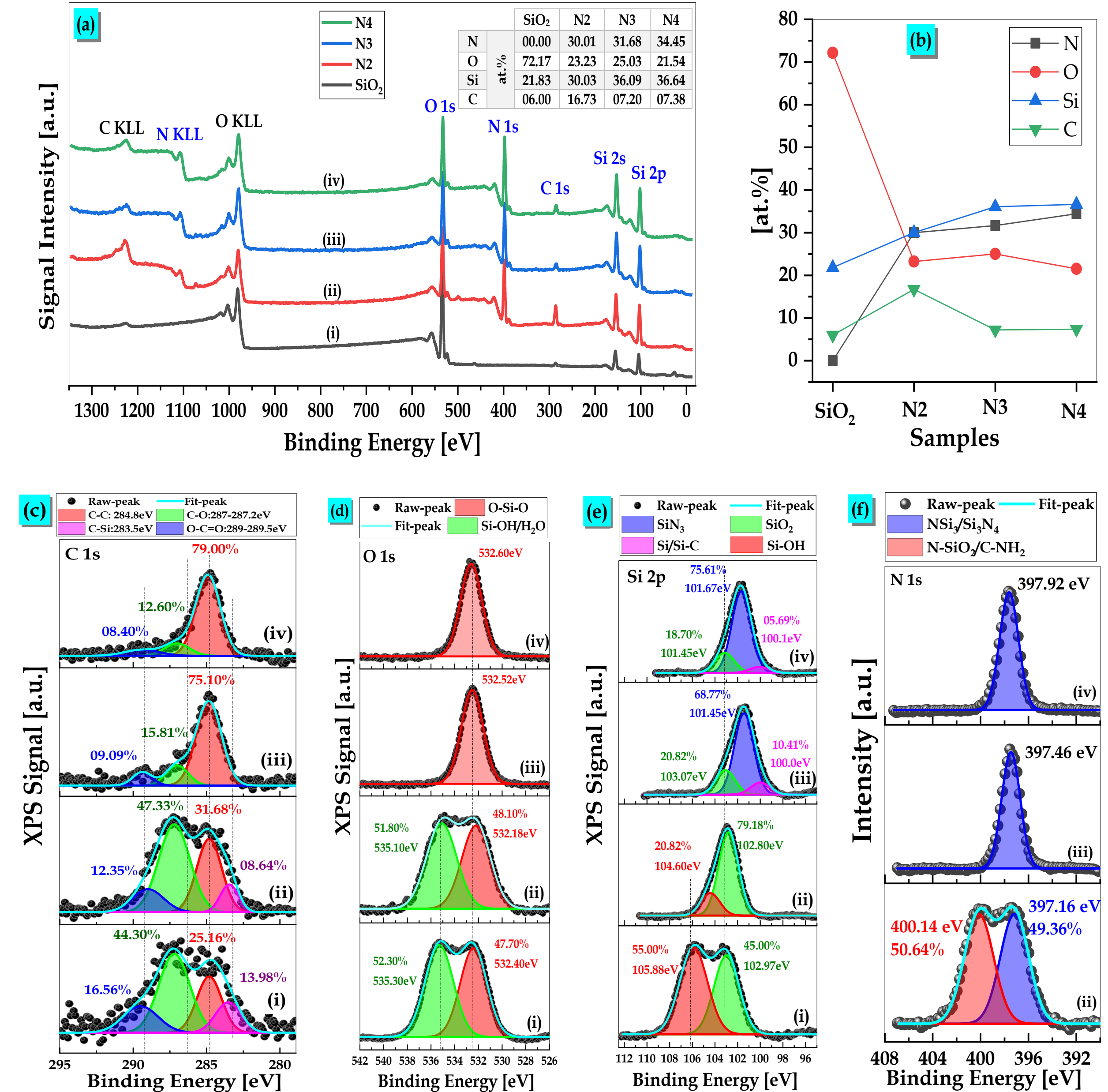

Fig. 5 – Elements analysis of Si_3N_4/SiO_2 films measured by XPS. (a) Spectra of SiO_2, N_2, N_3; and N_4. (b) Atomic percentages. (c) C peak. (d) O peak. (e) Si 2*p* peak. (f) N peak

Table 2 – Atomic percentage of elements analysis and recalculated taking into account the relative sensitive factor (RSF)

Samples	Atomic percentages [at.%]			
	Si	N	O	C
RSF	0.865	1.77	2.85	1
N1	3.4	/	95.50	1.11
N2	8.62	28.68	57	5.7
N3	9.91	28.98	58.77	2.34
N4	10.64	33.32	53.5	2.54

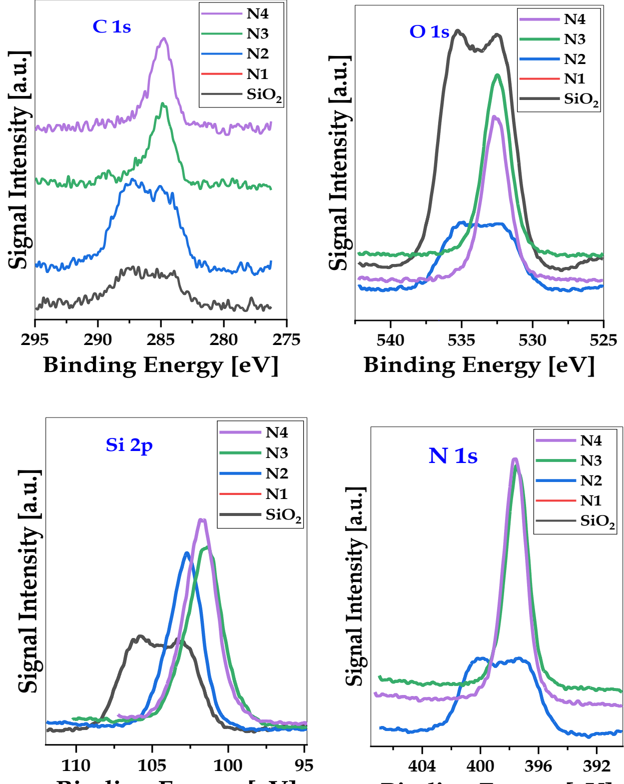

Fig. 6 – Elements (C 1*s*, O1*s*, Si 2*p* and N 1*s*) analysis of Si_3N_4 films measured by XPS

3.4 SEM Characterization

SEM analysis coupled with (EDS) and cross-sectional analysis, were performed to study the surface morphology. We assume that they are oxygen deposits or recrystallization with the help of microscopic analysis, disks whose diameter at the interface varies between 45 and 100 nm could be distinguished. Crystals of silicon [18, 20], formed by holding at 750 °C during the RTP anneal and solidified by rapid cooling during this process Fig. 7.

The intricacies of the surface morphologies are revealed by the SEM data; the growth on the SiN_x area is in fact a continuous film with a rough, grainy surface. SiN_x/SiO_2 structures that were deposited on silicon substrate are depicted in cross-section SEM images in Fig. 8.

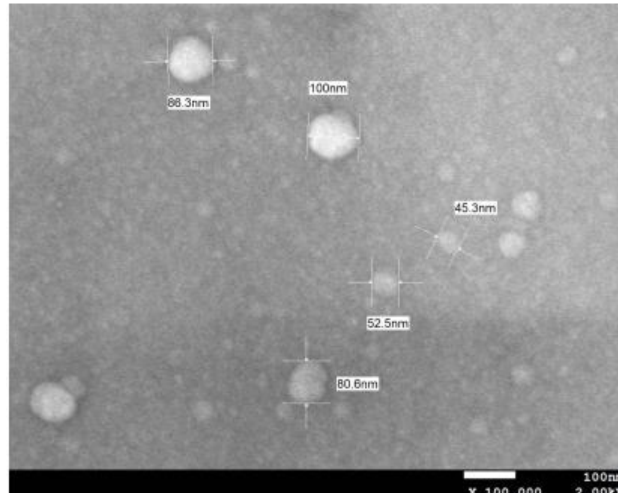

Fig. 7 – SEM image top view morphology of sample N_3

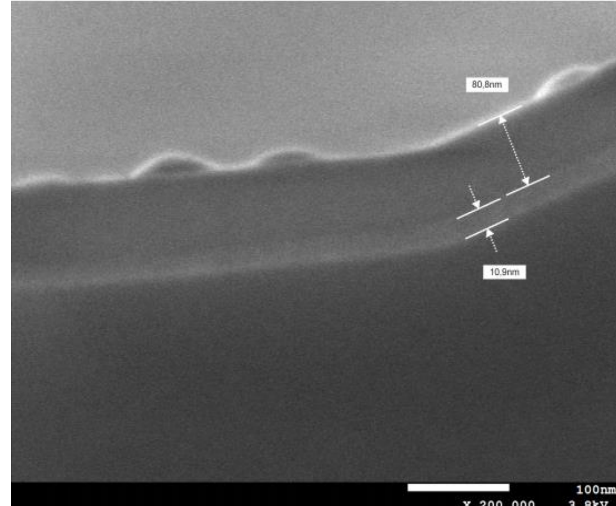

Fig. 8 – Cross-sectional SEM image of N_4

This is thought to be brought on by what is known as "blistering of the SiN_x layers," which is the layer's excessive hydrogen release during thermal annealing.

From de Fig. 7, we can conclude that the precipitated SiN_x and indicates that the porous layer deposition process is dependent on the silicon surface gas flow rate. Even while the EDS elemental analysis precision may not match that of XPS, it is nevertheless a faster and easier method of studying elemental composition. The EDS analysis confirmed the presence of Si, N, O, and C for all the samples prepared with different gas ratios, confirming the results calculated by XPS.

EDS analysis was used to confirm the presence of 65.48 % silicon 24.61 % nitrogen, 8.9 % oxygen, and 1.01 % carbon as shown in Fig. 9.

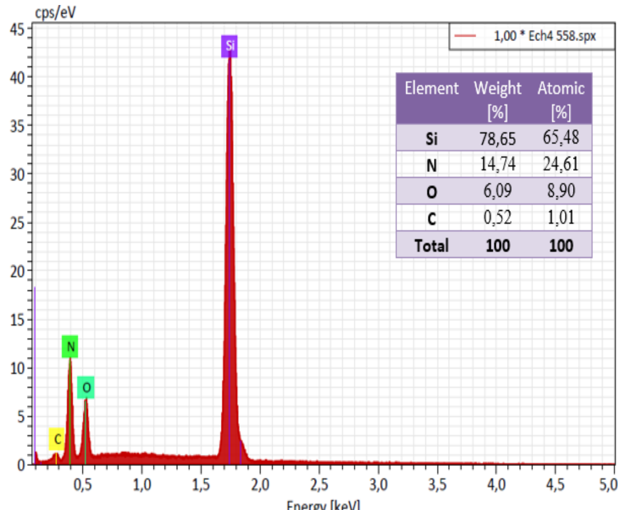

Fig. 9 – EDS images of the sample prepared N = 4

3.5 QSSC Characterization

The carrier lifetime is a crucial metric for measuring surface recombination. The lifetime can be determined using the photoconductance decay method by the WCT-120 Sinton lifetime tester. We examined the surface passivation after depositing the SiO_2 layer on *n*-type Cz-Si. Then, we investigated the coated SiN_x layer after overlaying it on the SiO_2 layer using QSSPC measurements.

Table 3 – Injection level effective minority carrier lifetime at 10^{15} cm^{-3}

Samples	V_{oc} (Volt)	J_0 (10^{-13}A/cm^2)	$\tau_{eff\,1}$ (10^{15}µs)	$\tau_{eff\,2}$ (10^{15}µs)	$\tau_{eff\,3}$ (10^{15}µs)
N1	0,6852	2,8919	281,91	241,44	333,74
N2	0,6852	2,7198	297,57	330,65	353,73
N3	0,6852	2,8764	230,83	79,39	313,86
N4	0.6851	4,8785	12,91	13,26	135,72

- τ_{eff1}: raised after oxidation;
- τ_{eff2}: reading after SiN_x passivation;
- τ_{eff3}: raised after RTP.

Table 3 shows the effective minority lifetimes for all samples of compensated *n*-type Cz silicon wafers. These results show that there can be a significant improvement in the minority charge carrier lifetime induced from adding passivation layers. Diffusion of hydrogen from the SiN_x layer into the silicon during the RTP stage is what causes this improvement in bulk lifetimes and its quality. A significant lifetime enhancement is seen following the deposition of SiN layers on the SiO_2. V_{oc} obtained with a SiN/SiO_2 is 680 mV, Hubner et al. confirm that SiN_x passivated cells with n^+-diffused emitters had attained open circuit voltages of 649 mV [20].

4. CONCLUSION

The optical and physicochemical characteristics of double-layer passivation coating made of (SiN_x/SiO_2) deposited on *n*-type monocrystalline silicon wafers deposited by thermal oxidation and PECVD, respectively, were thoroughly investigated. We primarily examined the effect of the ratio of the flow rates of the precursor gases $R = NH_3/SiH_4$ for their use in solar cell application, which we have varied between 4, 5, 6.5, and 8. Lifetime measurements used to assess the surface passivation quality of SiN_x deposited on thermally grown oxide on Si surface. The optical properties showed good anti-reflection properties for $R = 6.5$. It has been demonstrated that this PECVD technique, when used in conjunction with heat treatment after SiO_2 oxidation, can serve as an excellent AR coating and enhance the quality of the bulk silicon. The double layer passivation demonstrated a rise in the bulk life-time of minority charge carriers; it can wait more than 350 µs after RTP Annealing.

ACKNOWLEDGEMENTS

The authors would like to thank the General Directorate for Scientific Research and Technological Development (DGRST).

REFERENCES

1. E. Cornagliotti, A. Uruena, M. Aleman, A. Sharma, L. Tous, R. Russell, P. Choulat, J. Chen, J. John, M. Haslinger, F. Duerinckx, B. Dielissen, R. Gortzen, L. Black, J. Szlufci, *IEEE J. Photovoltaics* **5**, 1366 (2015).
2. A. El Amrani, A. Boucheham, A. Guendouzi, C. Nasraoui, R. Si-Kaddour, *Silicon* **14**, 223 (2022).
3. A. Rohatgi, P. Doshi, J. Moschner, T. Lauinger, A.G. Aberle, D.S. Ruby, *IEEE Trans. Electron Dev.* **47**, 987 (2000).
4. R.S. Bonilla, B. Hoex, P. Hamer, P.R. Wilshaw, *Phys. Status Solidi A* **214**, 7 (2017).
5. A. El Amrani, L. Boutaleb, A. Boucheham, Y. Belkacem, C. Nasraoui, *Mater. Res. Express* **5**, 015914 (2018).
6. S. Jafari, J. Hirsch, D. Lausch, M. John, N. Bernhard, S. Meyer, *AIP Conf. Proc.* **2147**, 050004 (2019).
7. D. Ding, G. Lu, Z. Li, Y. Zhang, W. Shen, *Sol. Energy* **193**, 494 (2019).
8. J. Benick, B. Hoex, G. Dingemans, W.M.M. Kessels, A. Richter, M. Hermle, S.W. Glunz, *24th European Photovoltaic Solar Energy Conf.* 863 (2009).
9. P.J. Cousins, D.D. Smith, H.-C. Luan, J. Manning, T.D. Dennis, A. Waldhauer, K.E. Wilson, G. Harley, W.P. Mulligan, *35th IEEE Photovoltaic Specialists Conf. (PVSC) (IEEE)*, 000275 (2010).
10. L.J. Geerligs, D. Macdonald, *Prog. Photovolt. Res. Appl.* **12** No 4, 309 (2004).
11. J.E. Cotter, J.H. Guo, P.J. Cousins, M.D. Abbott, F.W. Chen, K.C. Fisher, *IEEE Trans. Electron Dev.* **53**, 1893 (2006).
12. T. Lauinger, J. Moschner, A.G. Aberle, R. Hezel, *J. Vac. Sci.*

Technol. A **16**, 530 (1998).
13. C.-H. Yu, K.-A. Chiu, T.-H. Do, L. Chang, W.-C. Chen, *Coatings* **11** No 10, 1251 (2021).
14. N. Hegedüs, K. Balázsi, C. Balázsi, *Materials* **14**, 5658 (2021).
15. A.W. Weeber, H.C. Rieffe, I.G. Romijn, W.C. Sinke, W.J. Soppe, *Photovoltaic Specialists Conference. Conference Record of the 31st IEEE*, 1043 (2005).
16. R.A. Sinton, A. Cuevas, *Appl. Phys. Lett.* **69**, 2510 (1996).
17. S.D. Wolf, G. Agostinelli, G. Beaucarne, P. Vitanov, *J. Appl. Phys.* **97**, 063303 (2005).
18. S.D. Wolf, G. Agostinelli, G. Beaucarne, P. Vitanov, *Semicond. Sci. Technol.* **16**, 164 (2001).
19. T. Lauinger, J. Moschner, A.G. Aberle, R. Hezel, *J. Vac. Sci. Technol. A* **16**, 530 (1998).
20. Shih-Liang Ku, Cheng-Chung Lee, *Opt. Mater.* **32**, 956 (2010).

Вплив шарів пасивації SiN_x/SiO_2 на розсіяне поле поверхні в кремнієвих пластинах *n*-типу

B. Labdelli[1], A. Boucheham[1], L. Benharrat[1], A. Djelloul[1], N. Chahinez[1], M. Alloun[2], S.Y. Lamri[2]

[1] *Centre de Recherche en Technologie des Semi-Conducteurs pour l'Energétique 'CRTSE', Alger, Algérie*
[2] *École Nationale Polytechnique Département de Métallurgie, 16200 Alger, Algeria*

У роботі представлені результати досліджень властивостей пасивації пакету плівок нітриду кремнію (SiN_x) поверх діоксиду кремнію (SiO_2) на кремнієвих пластинах *n*-типу з метою вивчення його впливу на поле передньої поверхні (FSF) у сонячних елементах PERT. Кремнієві пластини пройшли ідентичний процес термічного окислення протягом 30 хвилин при 850 °C (10 нм) в печі для окислення. Матеріали SiN_x були нанесені за допомогою плазмово-посиленого хімічного осадження з парової фази (PECVD) на кремнієву підкладку *n*-типу, нітрид кремнію, де регулювали співвідношення газу-попередника (R = NH_3/SiN_4), потім використовували швидку термічну обробку (RTP) спільного спалювання при температурі 750 °C протягом 60 с. Де дифузії фосфору проводяться з використанням $POCl_3$ як джерела допанту при температурі 820 °C протягом 15 хвилин у трубчастій печі. Показник відбиття показує, що подвійні шари плівок SiN/SiO_2 у сонячних елементах забезпечують ефект антивідблиску, а хороша пасивація випромінювачів призводить до поліпшених електричних характеристик. Це було підтверджено за допомогою квазістаціонарної фотопровідності (QSSPC) Sinton WCT 120 із використанням $n^+/n/n^+$ симетричних зразків тривалості життя. Шари SiN_x, нанесені на SiO_2, демонструють ефективні характеристики пасивації об'єму та поверхні.

Ключові слова: SiN_x/SiO_2, PECVD, RTP, Монокристалічний кремній *n*-типу, QSSPC.